Catalytic and Structural Role of a Metal-Free Histidine Residue in Bovine Cu−Zn Superoxide Dismutase

Akira Toyama, Yohko Takahashi, and Hideo Takeuchi*

Graduate School of Pharmaceutical Sciences, Tohoku University, Aobayama, Sendai 980-8578, Japan

Received February 2, 2004; Revised Manuscript Received February 25, 2004

ABSTRACT: Cu−Zn superoxide dismutase (SOD) contains a conserved, metal-free His residue at an opening of the backbone β-barrel in addition to six Cu- and/or Zn-bound His residues in the active site. We examined the protonation and hydrogen bonding state of the metal-free His residue (His41) in bovine SOD by UV Raman spectroscopy. Analysis of the His Raman intensity at 1406 cm^{-1} in a D_2O solution has shown that His41 has a pK_a of 9.4, consistent with the NMR and X-ray structures at acidic to neutral pH, in which two imidazole nitrogen atoms of cationic His41 are hydrogen bonded to the main chain C═O groups of Thr37 and His118. Upon deprotonation of His41 at pH 9.4, the Thr37−His41−His118 hydrogen bond bridge breaks on the His118 side and SOD loses 70% of its activity. Concomitantly, hydrogen−deuterium exchange is accelerated for amide groups of β-strands, indicating an increased conformational fluctuation of the β-barrel. Thr37 and His41 are in direct contact with Leu36, whose hydrophobic side chain closes off the opening of the β-barrel, while His118 is indirectly connected to Arg141 that assists the docking of superoxide to Cu. These Raman findings strongly suggest that the His41-mediated hydrogen bond bridge plays a crucial role in keeping the protein structure suitable for highly efficient catalytic reactions. The catalytic and structural role of His41 is consistent with the observation that the mutation of His43 in human SOD (equivalent to His41 in bovine SOD) to Arg largely reduces the dismutase activity and the protein structural stability.

Cu−Zn superoxide dismutase (SOD)[1] is an enzyme that catalyzes the disproportionation of superoxide (O_2^-) into less reactive hydrogen peroxide and molecular oxygen ($2O_2^- + 2H^+ \rightarrow H_2O_2 + O_2$) (*1*−*3*). Superoxide radical anions are commonly produced by aerobic metabolism, and they can initiate radical chain reactions that damage cellular constituents such as lipids and proteins (*3*, *4*). Oxidative stress induced by uncontrolled production of superoxide and its reaction products is implicated in the pathogenesis of neurodegenerative disorders, cancer, and aging (*4*−*7*). SOD is abundantly found in the intracellular cytoplasmic space of aerobic organisms and plays a central role in protecting cells from oxidative stress (*5*−*7*). Because of its importance as an antioxidant enzyme, the structure and catalytic mechanism of SOD have been studied extensively by using biochemical, spectroscopic, and diffraction methods.

Bovine erythrocyte SOD, a representative of the SOD family, is a dimer of two identical subunits. The polypeptide chain of each subunit is composed of 151 amino acids and folded into an eight-stranded antiparallel β-barrel with three major external loops (*8*−*12*). The enzyme active site contains a pair of Cu and Zn ions surrounded by two major external loops beside the backbone β-barrel. The Cu and Zn ions are both divalent in the usual oxidized state and bridged by the anionic imidazole (imidazolate) ring of His61. The Cu ion is further coordinated by three His residues (His44, His46, and His118) with a water molecule at the apex of a distorted square pyramid. The Zn coordination is completed by three additional ligands (His69, His78, and Asp81) in a distorted tetrahedral geometry.

According to the currently accepted catalytic mechanism (*13*, *14*), the dismutation reaction of SOD involves alternate reduction and oxidation of the Cu ion during successive encounters with superoxide. In the reduction phase, the Cu(II) ion becomes Cu(I) by extracting an electron from a superoxide radical anion to produce molecular oxygen. Concomitantly, the His61 imidazolate bridge is broken on the Cu side and His61 gains a proton from the solvent (*15*−*18*). In the oxidation phase, the Cu(I) gives an electron to another superoxide anion, which receives two protons from His61 and the solvent to become hydrogen peroxide. Meanwhile, the His61−Cu(II) coordination is restored. The metal-bound His residues other than His61 play a structural role, and Arg141 on the rim of the active site docks superoxide to the Cu ion by using its positively charged side chain.

In addition to the unique active site structure and catalytic mechanism, SOD is characterized by an extremely high catalytic efficiency. The rate constant of superoxide dismutation is close to the theoretical diffusion limit over a wide pH range from 5 to 9, in particular at low ionic strengths

* To whom correspondence should be addressed. Phone or fax: +81-22-217-6855. E-mail: takeuchi@mail.tains.tohoku.ac.jp.

[1] Abbreviations: ALS, amyotrophic lateral sclerosis; FALS, familial amyotrophic lateral sclerosis; HisD, neutral histidine deuterated at an imidazole nitrogen atom; $HisD_2^+$, cationic histidine deuterated at both imidazole nitrogen atoms, Nπ and Nτ; His−M, neutral histidine bound to a metal ion via either Nπ or Nτ; $His^- - M_2$, anionic histidine bridging two metal ions; His Nπ−M, neutral histidine with Nπ−metal coordination; His Nτ−M, neutral histidine with Nτ−metal coordination; NBT, nitroblue tetrazolium; SOD, copper−zinc superoxide dismutase.

10.1021/bi049767k CCC: $27.50
Published on Web 04/01/2004

(*19*−*21*). To account for such a high catalytic efficiency, positively and negatively charged residues on the protein surface have been proposed to accelerate the catalytic reaction by guiding and steering superoxide toward the active site (*21*−*31*). Above pH 9, on the other hand, SOD shows a stepwise loss of activity, which appears around pH 9.5 and 11.5 (*28*−*30*). Although the transition at pH 11.5 is mostly ascribed to the deprotonation of Arg141 on the rim of the active site, the residues responsible for the deactivation at pH 9.5 are still controversial (*28*−*33*).

In this study, we have investigated the mechanism of deactivation at pH 9.5 by UV Raman spectroscopy with special attention to His41, which is one of the amino acid residues that is highly conserved in the SOD family (*34*) but not involved in the active site metal coordination (*8*−*12*). UV Raman spectroscopy is a useful tool for determining the ionization and hydrogen bonding states of His, especially in a D_2O solution (*35*−*39*). Analysis of UV Raman spectra of bovine SOD has confirmed that His41 is cationic at pD 5−9, as suggested by NMR and X-ray structures, in which two imidazole nitrogen atoms of His41 are hydrogen bonded to the main chain C═O groups of Thr37 and His118 (*8*−*10*, *40*). Examination of the pD dependence of UV Raman spectra has further revealed that the Thr37−His41−His118 hydrogen bond bridge is disrupted on the His118 side at pD 9.4, where SOD loses most of its activity. Concomitantly, hydrogen−deuterium (H−D) exchange is accelerated for amide protons of the β-barrel, indicating an increased fluctuation of the β-barrel structure. The His41-mediated hydrogen bond bridge is further extended to Leu36, whose hydrophobic side chain closes off an opening of the β-barrel, and to Arg141, which is thought to dock superoxide to the Cu site (*8*−*10*). The Raman findings presented here strongly suggest that His41 plays an important role in maintaining the high catalytic efficiency of SOD by forming a hydrogen bond bridge that indirectly connects the structurally important Leu36 and catalytically important Arg141 residues.

MATERIALS AND METHODS

Sample Preparation and Activity Assay. SOD was isolated from bovine erythrocytes and purified according to the procedure of McCord and Fridovich (*5*), followed by additional purification by gel exclusion chromatography on a Sephacryl S-200 column (Pharmacia). The pH dependence of the catalytic activity was examined with an inhibition assay of the reduction of nitroblue tetrazolium (NBT) by superoxide, which was produced by xanthine oxidase from xanthine and oxygen (*41*). The concentration of xanthine oxidase in the reaction mixture was adjusted so that the rate of NBT reduction monitored at 560 nm could be close to a constant value at every pH. The activity of SOD was determined by the amount of enzyme required to halve the rate of NBT reduction. The buffers that were used were 20 mM NaH_2PO_4/Na_2HPO_4 (pH 7−8), H_3BO_3/NaOH (pH 8.5), Gly/NaOH (pH 9−10.5), and Na_2HPO_4/NaOH (pH 11). All buffer solutions were supplemented with 0.1 mM ethylenediaminetetraacetic acid for scavenging adventitious free divalent metal cations that might interfere with the activity assay. NaCl was also added at a concentration of 150 mM to keep the ionic strength nearly constant around a physiological level in all assay solutions. Activity assays were performed five or six times with freshly prepared samples.

Acquisition of UV Raman Spectra. Since structural marker Raman bands of His are more discernible for the N-deuterated imidazole ring than for the N-hydrated ring (*35*−*39*), Raman samples of SOD were prepared in D_2O buffer solutions: CH_3COOD/CH_3COONa (pD 5), NaD_2PO_4/Na_2DPO_4 (pD 6−8), Gly/NaOD (pD 8.5−10), and Na_2DPO_4/NaOD (pD 11). All the buffer solutions were prepared at a concentration of 20 mM, and the ionic strength was increased by adding NaCl and $NaClO_4$ (75 mM each). The 934 cm^{-1} Raman band of ClO_4^- was used as an internal standard of Raman intensity. The concentration of the enzyme was 0.2 mM as determined with an extinction coefficient of 10 300 M^{-1} cm^{-1} at 258 nm (*5*). Solution samples of amino acids Tyr (1.5 mM), Phe (50 mM), and His (50 mM) were prepared in D_2O, and the pD values of the solutions were adjusted with DCl and NaOD. For His, H_2O solution samples were also prepared in a similar way.

UV Raman spectra were excited at 229 nm by using continuous-wave radiation from an intracavity frequency-doubled Ar^+ ion laser (Coherent Innova, model 300 FReD) and recorded on a UV Raman spectrometer (Jasco, model TR-600UV) equipped with a liquid nitrogen-cooled CCD detector (Princeton Instruments, model LN/CCD-1152). The sample solution was spun in a spinning quartz cell, and the laser power was 1−5 mW at the sample. Typically, Raman spectra were recorded with an accumulation time of 30−80 min, and three or more spectra recorded on fresh samples were averaged. Sample integrity was verified by the observation of the same absorption spectrum (typical of the active enzyme) before and after laser irradiation. Wavenumber calibration was effected by using the Raman spectrum of a cyclohexanone/acetonitrile mixture (1:1, v/v), and peak wavenumbers of sharp Raman bands were reproducible to within ± 1 cm^{-1}. Overlapping Raman bands were resolved by assuming a Voigt profile (a convolution of a Gauss and a Lorentz profile) for each component band (*42*, *43*). Laboratory-made software was used for the curve fitting computations.

RESULTS

Catalytic Activity. Previous studies employing various assay methods and solution conditions reported that the catalytic activity of SOD was almost constant in the pH range of 5−9 (*19*−*21*) and underwent a significant drop around pH 9.5 (*28*−*30*). To assess whether the corresponding alkaline deactivation occurs at physiological ionic strength, we assayed the activity of bovine SOD at varied pH values in the presence of 150 mM NaCl. Figure 1 shows the pH dependence of the activity measured relative to that at pH 8.0. When the pH is increased from 8 to 11, the enzyme loses ~70% of its activity with a transition midpoint at pH 9.5. This transition is analogous to that reported previously for bovine and other eukaryotic SODs at lower ionic strengths (*28*−*30*). This assay confirms that the activity of SOD drops at pH 9.5 under the conditions of physiological ionic strength as well. Since the deactivation may be linked with deprotonation of one or more specific amino acid residues, UV Raman spectra of SOD were examined to reveal the chemical species that releases a proton around pH 9.5.

Assignments of UV Raman Bands. Figure 2 shows the UV (229 nm) Raman spectrum of bovine SOD in a D_2O solution

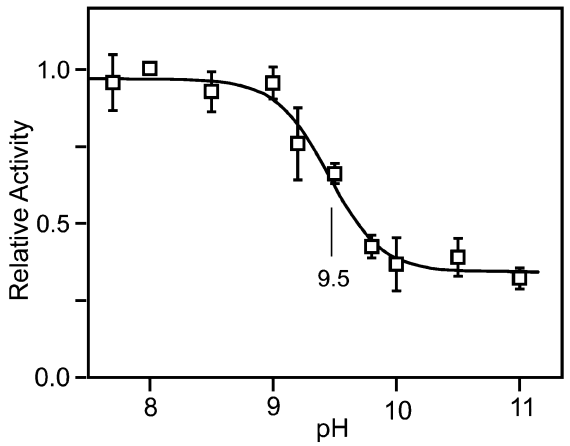

FIGURE 1: Catalytic activity of bovine SOD plotted as a function of pH. The activity was measured by the NBT method in the presence of 150 mM NaCl and normalized to that at pH 8.0. The plot shows the mean and standard deviation of five or six experiments. The pH at the midpoint of the transition (9.5) is indicated with a thin vertical bar.

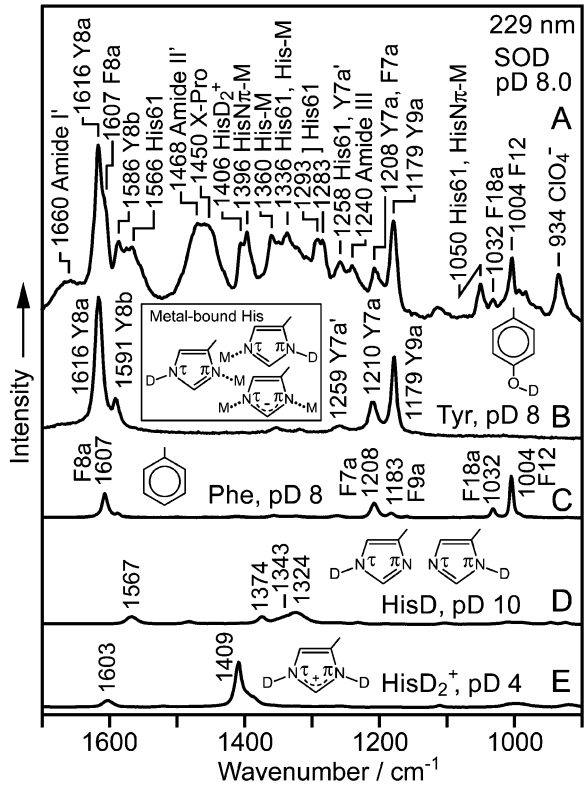

FIGURE 2: UV (229 nm) Raman spectrum of (A) 0.2 mM SOD at pD 8.0 compared with those of (B) Tyr at pD 8, (C) Phe at pD 8, (D) His at pD 10, and (E) His at pD 4. The amino acid concentration was 1.5 mM for Tyr and 50 mM for Phe and His. The 934 cm^{-1} band in the SOD Raman spectrum is due to 75 mM ClO_4^-, added as an internal intensity standard. See the text for the assignments of the other Raman bands. Three forms of metal-bound His are illustrated in the inset.

at pD 8.0 (A) together with those of amino acids Tyr (B), Phe (C), and His (D and E). SOD contains one Tyr, four Phe, and eight His residues per subunit. By comparison of with the Raman spectra of amino acids, the 1616, 1586, and 1179 cm^{-1} bands of SOD are assigned to the Y8a, Y8b, and Y9a vibrations of Tyr, respectively (*44*, *45*). Part of the 1258 cm^{-1} intensity may arise from the Y7a′ mode of Tyr. The 1208 cm^{-1} band is also attributed to Tyr (Y7a) with a small contribution from the F7a mode of Phe (*44*, *45*). Raman bands due to solely Phe are seen at 1607 (F8a), 1032 (F18a), and 1004 cm^{-1} (F12).

In the active site of SOD, three His residues (His44, His46, and His118) are bound to Cu(II), two (His69 and His78) are ligated to Zn(II), and one (His61) bridges Cu(II) and Zn(II) (*8*−*12*). Of the two nitrogen atoms on the imidazole ring, Nπ is the metal binding site in His44, His69, and His78 (His Nπ−M), while the Nτ atom coordinates to the metal in His46 and His118 (His Nτ−M). His61 has an anionic imidazolate ring with Nπ−Zn(II) and Nτ−Cu(II) coordination (His^-−M_2). Since the imidazolate bridge of His61 is broken on the Cu side in the reduced state (*15*−*17*), the Raman bands due to His61 are readily identified by changes associated with the His^-−M_2 → His Nπ−M conversion. In previous UV Raman studies on SOD (*18*, *46*−*48*), a singlet at 1566 cm^{-1} and a doublet at 1293/1283 cm^{-1} disappeared upon reduction of the enzyme, and they were unequivocally assigned to His61 (Figure 2A). Three bands at 1336, 1258, and 1050 cm^{-1} decreased in intensity in the reduced state, suggesting a contribution from His61 (*18*, *48*). Studies on model compounds and Cu- and/or Zn-depleted SOD in D_2O solution revealed some Raman bands characteristic of His residues bound to a single metal ion (His−M) (*18*, *47*, *48*). Contributions of His−M were proposed for the 1360 and 1336 cm^{-1} bands, while the 1396 cm^{-1} band was more specifically attributed to His Nπ−M (*18*, *48*). The 1050 cm^{-1} band was also suggested to have a contribution from His Nπ−M (*48*).

In addition to the metal-bound His residues in the active site, SOD contains two metal-free His residues, which are located far from (His19) or in the vicinity of the active site (His41) (*8*−*12*). However, Raman signals from His19 and His41 have not yet been identified in UV Raman spectra of SOD. Metal-free His is expected to be in equilibrium between neutral imidazole (HisD in D_2O) and cationic imidazolium ($HisD_2^+$ in D_2O) with a pK_a value dependent on the environment (pK_a ∼ 6.5 for the aqueous amino acid His). Here we propose that the 1406 cm^{-1} shoulder band of SOD at pD 8.0 (Figure 2A) is due to the $HisD_2^+$ form of His19 and/or His41 because the shoulder band is observed in only the D_2O solution, its wavenumber is nearly identical to that (1409 cm^{-1}) found in the Raman spectrum of amino acid His at pD 4.0 (Figure 2E), and its intensity decreases with an increase in the pD of the SOD solution (see below).

Peptide main chain vibrations also exhibit several Raman bands in the D_2O solution spectrum of SOD (Figure 2A). The bands at 1660 and 1468 cm^{-1} are assigned to the amide I′ and II′ modes, respectively, of N-deuterated amide groups (*44*, *45*). SOD contains six Pro residues per subunit, and the 1450 cm^{-1} shoulder peak is ascribed to the imide C═O stretch of the X−Pro linkage on the basis of its insensitivity to the H_2O → D_2O solvent change (*18*, *48*). Previous Raman studies reported that a band at 1240 cm^{-1} characteristic of β-sheet structure appeared strongly in the H_2O solution but disappeared after prolonged incubation in D_2O (*18*, *48*). The 1240 cm^{-1} band in Figure 2A is thus ascribed to the amide III vibration of nondeuterated β-strands in the β-barrel (*44*, *45*, *49*). This assignment is consistent with the NMR observation that H−D exchange is very slow in the β-barrel domain (*40*). Solvent D_2O molecules may be hardly accessible to the amide groups in the β-barrel, at least at pD 8.0.

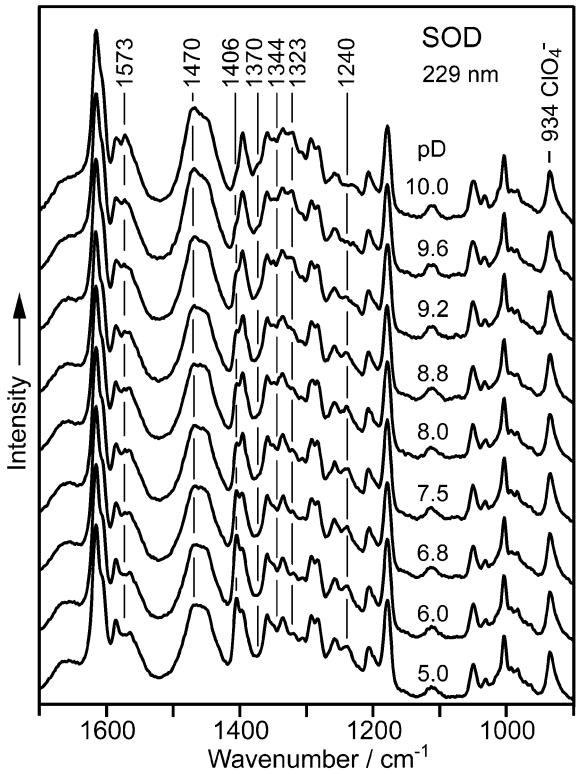

FIGURE 3: Effect of pD on the UV (229 nm) Raman spectrum of SOD. The SOD concentration was 0.2 mM, and the pD value was varied by using different buffer solutions containing NaCl and $NaClO_4$ (75 mM each). The 934 cm^{-1} band of ClO_4^- was used as an internal intensity standard. Vertical lines indicate the wavenumber positions of marked intensity changes.

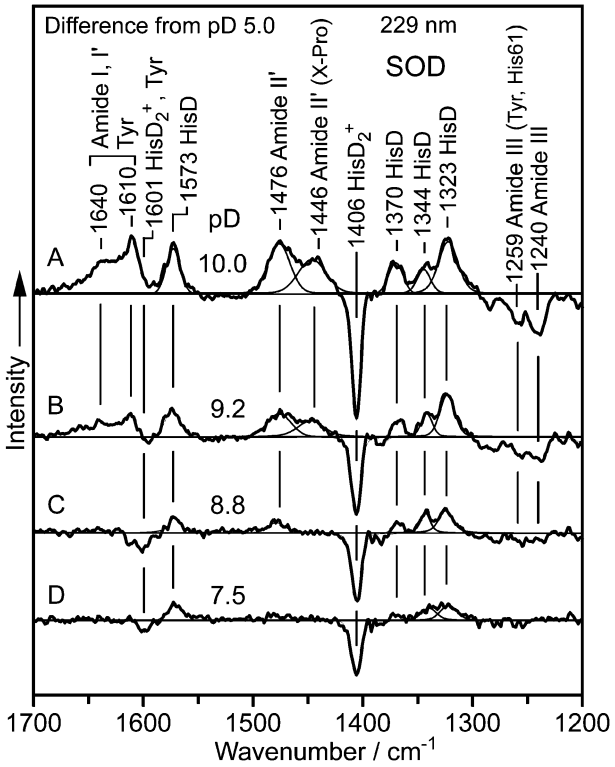

FIGURE 4: Difference Raman spectra of SOD demonstrating the effect of pD. The Raman spectrum at pD 5.0 was subtracted from those at pD (A) 10.0, (B) 9.2, (C) 8.8, and (D) 7.5. The original UV Raman spectra used in the difference calculations are shown in Figure 3. The positive and negative bands indicate intensity increases and decreases, respectively, associated with an increase of pD from 5.0 to the indicated value. The difference spectra in the 1600−1300 cm^{-1} region were decomposed into component bands of Voigt profiles as indicated with thin lines.

pD Dependence of the UV Raman Spectrum. Figure 3 compares UV Raman spectra of SOD in D_2O solutions at pD 5.0−10.0. Marked effects of pD change are seen at the following wavenumber positions. The prominent peak at 1406 cm^{-1} in the pD 5.0 Raman spectrum decreases in intensity with an increase in pD and finally disappears at pD 10.0. Concomitantly, peaks grow at 1573 and 1323 cm^{-1}. Similar but smaller growth is seen at 1370 and 1344 cm^{-1}. The 1240 cm^{-1} amide III band of nondeuterated β-strands starts to lose intensity above pD 8.8, and instead, a peak grows around 1470 cm^{-1}. In contrast to these pD-dependent changes, the Raman bands assigned to metal-bound His in Figure 2A do not show any significant change, indicating no structural alternation for the Cu(II)- and Zn(II)-bound His residues in the active site throughout the pD range of 5.0−10.0. Structural changes in other regions of the protein must be responsible for the observed pD dependence of the Raman spectrum.

Difference Raman Spectra. To analyze the Raman spectral changes more precisely, we have subtracted the spectrum at pD 5.0 from those at other pD values. Figure 4 shows such difference spectra at pD 7.5, 8.8, 9.2, and 10.0. The negative band at 1240 cm^{-1} in the difference spectrum at pD 10.0 is assigned to the amide III mode of the nondeuterated β-barrel as described above. An accompanying positive band at 1476 cm^{-1} is ascribed primarily to the amide II′ mode of N-deuterated main chain segments on the basis of its wavenumber and intensity behavior (*44*, *45*). The negative and positive band pair at 1240 and 1476 cm^{-1}, respectively, is prominent only above pD 9, suggesting that the amide protons of the β-barrel are highly shielded from solvent below pD 9 (Figure 4A,B). Generally, amide H−D exchange is accelerated at alkaline pD by base-catalyzed mechanisms if D_2O and OD^- are accessible to the exchange site (*49*). The rapid growth of the 1240 and 1476 cm^{-1} band pair above pD 9 is thus indicative of an increase in solvent accessibility that facilitates base-catalyzed exchange reactions. The β-barrel is likely to experience a significant conformational fluctuation above pD 9.

Another pair of negative and positive bands is seen at 1259 and 1446 cm^{-1}, respectively, in the difference spectra at pD 9.2 and 10.0 (Figure 4A,B). Although His61, Tyr108, and six Pro residues have Raman bands at these wavenumber positions (Figure 2A), part of the 1259 cm^{-1} intensity might be ascribed to the amide III mode of tight β-turns that are another structural element characterizing loop regions in SOD (*8*, *44*, *45*, *50*). Slowly exchanging amide protons have been identified by NMR spectroscopy in a loop containing tight β-turns as well as in the β-barrel domain (*40*).

The main features of the difference Raman spectra in Figure 4 can be assigned to metal-free His residues. The strong and sharp negative band at 1406 cm^{-1}, which becomes larger at higher pD values, indicates loss of N-deuterated cationic His ($HisD_2^+$). Another negative peak at 1601 cm^{-1} in the difference spectra at pD 7.5 and 8.8 is also ascribed to $HisD_2^+$ by comparison with the amino acid His Raman spectrum in Figure 2E. Above pD 9, however, no significant difference signal is seen at 1601 cm^{-1}. An overlap of a Tyr

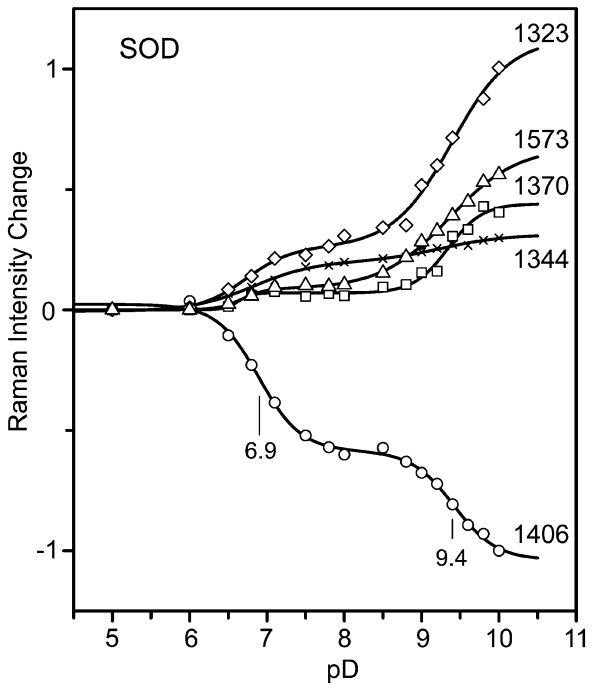

FIGURE 5: Intensities of His Raman bands of SOD plotted as a function of pD. The integrated intensities of the 1573, 1406, 1370, 1344, and 1323 cm^{-1} bands were computed by decomposing the difference spectra into component bands as shown in Figure 4. The intensities that were obtained were then normalized to that of the 1406 cm^{-1} band at pD 10.0. Since the difference spectra were calculated against the pD 5.0 spectrum, this figure shows the change in intensity from that at pD 5.0. The transition points at pD 6.9 and 9.4 are indicated with vertical bars.

positive band may account for the disappearance of the 1601 cm^{-1} negative band (see below). Below 1600 cm^{-1}, four positive bands grow at 1573, 1370, 1344, and 1323 cm^{-1} with an increase in pD (Figures 3 and 4). These positive bands can all be assigned to N-deuterated neutral His (HisD) because the Raman spectrum of amino acid His at pD 10 exhibits the corresponding bands at nearly identical wavenumber positions (Figure 2D). The pD dependence of the His Raman bands of SOD in Figure 4 clearly demonstrates that one or more His residues are converted from $HisD_2^+$ to HisD over a pD range from 5.0 to 10.0.

Above 1600 cm^{-1}, the difference Raman spectrum contains contributions from Tyr and main chain amide modes in addition to the 1601 cm^{-1} band of $HisD_2^+$ mentioned above. The Tyr Y8a band at 1616 cm^{-1} is strongly enhanced in the UV Raman spectrum (Figures 2B) and shifts to 1603 cm^{-1} upon deprotonation (*44*, *45*). The single Tyr residue (Tyr108) of bovine SOD has a pK_a of 11.4, and a small percent of Tyr108 is deprotonated at pD 10.0 (*48*). Accordingly, positive and negative bands are expected around 1603 and 1616 cm^{-1}, respectively, in the pH 10 difference spectrum. However, the former positive band may overlap the 1601 cm^{-1} negative band of $HisD_2^+$, while the latter negative band would be further overlapped by difference signals caused by a downshift and intensification of the amide I band upon N-deuteration (*44*, *45*). Because of such complicated overlap, the difference features above 1600 cm^{-1} are not amenable to further analysis. On the other hand, quantitative analysis of the difference spectra below 1600 cm^{-1} is expected to provide structural information about metal-free His residues.

Intensity Changes of His Raman Bands. The difference Raman spectra in the 1600−1300 cm^{-1} region were decomposed into component bands with Voigt function profiles as shown with thin lines in Figure 4. In Figure 5, the integrated intensity of each Raman band assigned to metal-free His is plotted as a function of pD, and the pD dependence is approximated by a sigmoid curve representing a Hill equation with one or two transition points (*51*, *52*). The 1406 cm^{-1} negative band reflecting the $HisD_2^+ \rightarrow$ HisD conversion exhibits two transitions with a comparable intensity change at pD 6.9 and 9.4 (Figure 5). SOD contains two metal-free His residues (His19 and His41) that can take the $HisD_2^+$ form. The pK_a of His19 has been found to be 6.7, and that of His41 is suggested to be above 9 by NMR spectroscopy (*53*, *54*). Thus, the first transition of the 1406 cm^{-1} intensity at pD 6.9 is ascribed to His19 and the second one at pD 9.4 to His41.

When $HisD_2^+$ is changed to HisD, the C4═C5 stretch mode of the imidazole ring shifts from ∼1600 to ∼1570 cm^{-1} (Figure 2D,E). The positive band at 1573 cm^{-1} in Figure 4 is ascribed to the C4═C5 stretch mode of His19 and His41 in the HisD form, and its intensity is expected to change comparably at pD 6.9 (His19) and 9.4 (His41), as observed for the 1406 cm^{-1} band. Actually, however, the 1573 cm^{-1} intensity shows a small change at pD 6.9 and a large change at pD 9.4 (Figure 5). Below pD 9, the 1573 cm^{-1} positive component seems to be partially overlapped by the negative component at 1601 cm^{-1} because of the C4═C5 stretch mode of $HisD_2^+$, leading to underestimation of the 1573 cm^{-1} intensity (Figure 4). Above pD 9, on the other hand, the influence of the 1601 cm^{-1} negative component is canceled out by another overlapping positive band due to Tyr108 as described above. This may be the reason the 1573 cm^{-1} intensity exhibits a smaller transition at pD 6.9 than at pD 9.4.

A large intensity increase is seen at pD 9.4 for the 1323 cm^{-1} band (Figure 5). This band also exhibits a smaller but significant intensity increase at pD 6.9, indicating contributions from both His19 and His41. Another band at 1370 cm^{-1} exhibits a pD dependence analogous to that of the 1323 cm^{-1} band and is again ascribed to His19 and His41. On the other hand, the 1344 cm^{-1} band exhibits a transition only at pD 6.9 (Figure 5), demonstrating that His19, but not His41, is responsible for the 1344 cm^{-1} band. In other words, His19 gives all three Raman bands at 1370, 1344, and 1323 cm^{-1}, whereas His41 produces only two of them at 1370 and 1323 cm^{-1}. The difference in Raman spectral properties between His19 and His41 may be related to the tautomerism of the imidazole ring.

Tautomeric States of His19 and His41. The neutral imidazole ring of His carries a proton (deuteron) on either of the two nitrogen atoms (Nτ and Nπ), and therefore, two tautomers (Nτ−H and Nπ−H or Nτ−D and Nπ−D) can exist. Itabashi and Itoh (*55*) examined Raman spectra of amino acid His in a D_2O solution with visible laser excitation and found two pairs of Nτ−D and Nπ−D tautomer markers at 1278 and 1258 cm^{-1} and at 995 and 1011 cm^{-1}, respectively, by utilizing the pD dependence of the tautomeric equilibrium. This was possible because the tautomeric equilibrium of amino acid His is affected by the ionization state of the amino group. In an H_2O solution, the C4═C5 stretch mode is sensitive to the tautomerism because of a

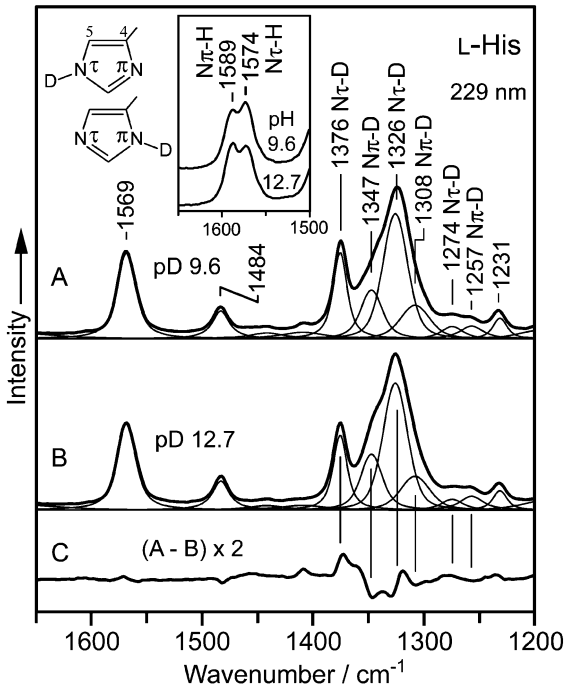

FIGURE 6: UV (229 nm) Raman spectra of amino acid His at pD (A) 9.6 and (B) 12.7. Trace C shows the difference spectrum (A − B) amplified twice. The corresponding Raman spectra in H_2O solutions at pH 9.6 and 12.7 are shown in the inset. The thin lines in traces A and B indicate the result of band decomposition with Voigt profiles. Tautomer Raman markers are labeled with Nπ−D (Nπ−H) and Nτ−D (Nπ−H).

coupling with the N−H bend. The Nπ−H tautomer gives a C4═C5 stretch band at ∼1590 cm^{-1}, while the corresponding band of the Nτ−H tautomer appears at ∼1575 cm^{-1} (*39*, *56*). The inset of Figure 6 shows the UV (229 nm) Raman spectra of amino acid His at pH 9.6 and 12.7 in the C4═C5 stretch region. The 1589 cm^{-1} band gains intensity compared to the 1574 cm^{-1} band on going from pH 9.6 to 12.7, demonstrating that the Nπ−H form is favored in a very basic solution.

In a D_2O solution, the C4═C5 stretch mode loses the tautomer sensitivity, but other vibrations become sensitive to tautomerism. Traces A and B of Figure 6 are the UV (229 nm) Raman spectra of amino acid His at pD 9.6 and 12.7, respectively. Trace C shows the difference (A − B), where the positive and negative peaks indicate the wavenumber positions of the Nτ−D and Nπ−D tautomer bands, respectively (the derivative-like features in the difference spectrum are due to small shifts in the peak wavenumber). Decomposition of the Raman spectra at pD 9.6 and 12.7 with Voigt function profiles reveals new marker bands at 1376 and 1326 cm^{-1}, respectively, for the Nτ−D tautomer and those at 1347 and 1308 cm^{-1}, respectively, for the Nπ−D tautomer as indicated with thin lines in traces A and B of Figure 6. The weak UV Raman bands at 1274 (Nτ−D) and 1257 cm^{-1} (Nπ−D) correspond to the 1278 and 1258 cm^{-1} visible Raman markers, respectively, reported previously by Itabashi and Itoh (*55*).

On the basis of the tautomer marker bands of amino acid His (Figure 6), the 1344 cm^{-1} band in the SOD difference spectra in Figure 4 is assigned to His residues in the Nπ−D form, while the 1370 and 1323 cm^{-1} bands are ascribed to the Nτ−D form. All the 1370, 1344, and 1323 cm^{-1} bands increased in intensity upon deprotonation of His19 at pD 6.9 (Figure 5). This observation indicates that His19 takes both the Nπ−D and Nτ−D forms above pD 6.9. The coexistence of two tautomers for His19 is consistent with the X-ray crystallographic finding that the imidazole ring of His19 is fully exposed to the solvent and neither imidazole nitrogen atom is hydrogen bonded to a specific part of the protein (*8*−*12*). His19 is not conserved in the SOD family and is thought to be functionally unimportant (*34*).

In contrast to His19, the $HisD_2^+ \rightarrow$ HisD conversion of His41 at pD 9.4 produces a significant intensity increase only for the Nτ−D tautomer markers at 1370 and 1323 cm^{-1} (Figure 5). According to the X-ray and NMR structures (*8*−*10*, *40*), the imidazole ring of His41 is involved in two hydrogen bonds at acidic to neutral pH. One is an Nτ−H···O bond with the main chain C═O group of Thr37, and the other is an Nπ−H···O bond with the main chain C═O group of His118. The existence of only the Nτ−D tautomer above pD 9.4 indicates that deprotonation occurs at Nπ, and therefore, His41 is no longer hydrogen-bonded with His118. These Raman data show that the Thr37−His41−His118 hydrogen bond bridge breaks on the His118 side at pD 9.4, where SOD loses most of its catalytic activity. Since His41 is highly conserved among eukaryotic and prokaryotic SODs (*34*), the hydrogen bonding state of His41 must be functionally important.

DISCUSSION

SOD contains seven conserved His residues (*34*). Six of them are bound to Cu and/or Zn in the active site. The remaining one is located behind the active site without binding to the metal ions. Although the structure of the active site, including the metal-bound His residues, has been studied extensively, little attention has been paid to the metal-free His residue outside the active site. We have investigated the protonation and hydrogen bonding state of the metal-free His residue (His41) in bovine SOD by UV Raman spectroscopy. Analysis of UV Raman spectra has shown that the His41 imidazole ring releases a proton and the His41-mediated hydrogen bond bridge is broken in conjunction with a substantial loss of catalytic activity. This observation strongly suggests that His41 is an important part of the highly efficient catalytic machinery of SOD.

pK_a of His41. Previous NMR studies attempted to determine the pK_a value of His41 (or the equivalent His43 residue in human SOD) but only found that His41 did not titrate between pH 5 and 9 (*53*, *57*). A recent two-dimensional NMR study has shown that His41 is cationic at pH 5 and both nitrogen atoms on the imidazole ring are protonated and hydrogen bonded to the main chain C═O groups of Thr37 and His118 (Thr39 and His120 in human SOD, respectively) (*40*). The Thr37−His41−His118 hydrogen bond bridge in the NMR structure is also seen in the X-ray crystal structures of bovine and human SODs at pH 5−7.5 (*8*−*10*, *58*, *59*). The UV Raman spectra of bovine SOD presented here have shown that His41 titrates with a pK_a of 9.4. Although the pK_a of His41 obtained here is consistent with the previous NMR observation, it is unusually high compared to that of amino acid His in aqueous solution (∼6.5) or of solvent-exposed His19 in SOD (6.9). The unusually high pK_a value of His41 may have a structural origin and functional relevance.

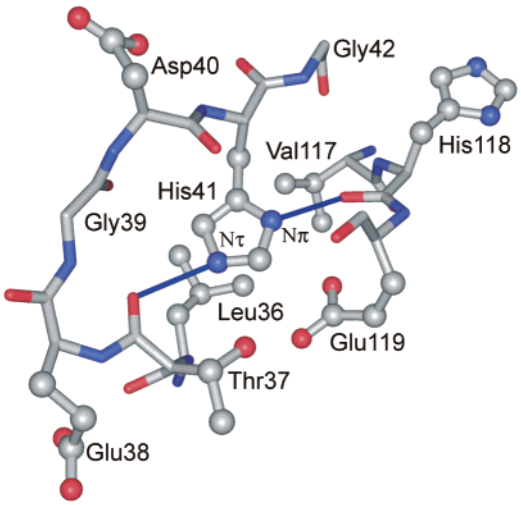

FIGURE 7: Environment of His41 in the crystal structure of bovine SOD viewed from the protein surface (*8*). The atomic coordinates were taken from those of subunit B in the X-ray crystal structure (Protein Data Bank entry 2SOD). The side chain atoms are shown as balls and the main chain atoms as sticks. Blue thin sticks represent the hydrogen bonds of His41.

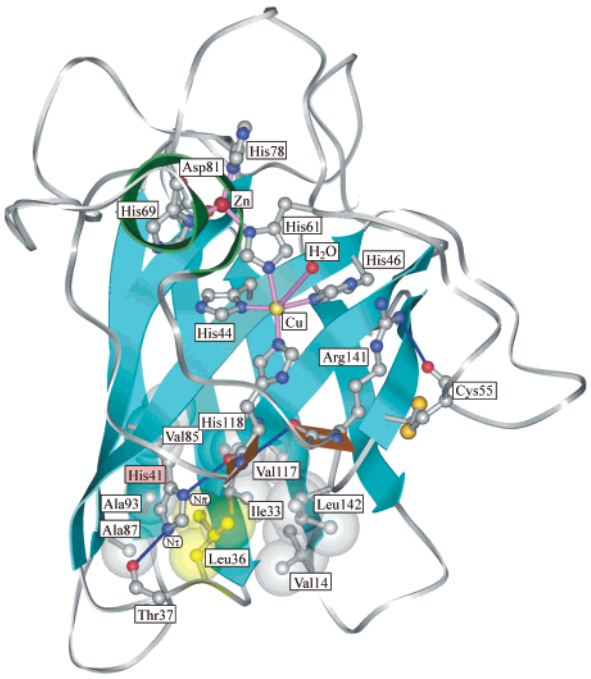

FIGURE 8: Subunit structure of bovine SOD (*8*). The atomic coordinates were taken from those of subunit B in the X-ray crystal structure of bovine SOD (Protein Data Bank entry 2SOD). The side chains are shown for the residues in the active site, on the rim of the active site pocket, and at an opening of the β-barrel near His41. For the hydrophobic residues closing off the β-barrel opening, transparent balls with van der Waals radii are superimposed on the ball-and-stick model. The central hydrophobic plug Leu38 is colored yellow. Blue thin sticks represent hydrogen bonds, and brown plates represent amide planes.

Environmental factors such as electrostatic interactions, hydrogen bonding, and shielding from the solvent affect the pK_a value of a His residue in the protein (*60*). Figure 7 shows the environment of His41 in the X-ray crystal structure of bovine SOD viewed from the protein surface (*8*). The side chain imidazole ring of His41 is half-buried in the protein and surrounded by three COO^- groups of Glu38, Asp40, and Glu119, which all favor the fully protonated cationic state of the His41 imidazole ring. The oxygen atoms of the Thr37 side chain and of the main chain C═O groups of Gly39, Asp40, and Glu119 are located within 3.5 Å of the imidazole ring, and their partial negative charges are likely to provide additional stabilization for the cationic state of His41. The main chain C═O groups of Thr37 and His118 are spatially arranged to be hydrogen bonded with the imidazole Nτ and Nπ atoms of His41, respectively, and the hydrogen bonds once formed at both nitrogen atoms would disfavor release of a proton from either of the nitrogen atoms. All these environmental factors are likely to contribute to the unusually high pK_a of His41, which makes it possible for His41 to form the Thr37−His41−His118 hydrogen bond bridge over a wide pH range from acidic to basic. Another enzyme, protein tyrosine phosphatase, also contains an unusual His residue, which is located in a negatively charged environment, is titrated at pH 9.2, and plays an important role in maintaining the active site structure of the enzyme (*61*).

Catalytic and Structural Role of His41. SOD loses ~70% of its catalytic activity at pH 9.5, which is concomitant with the disruption of the Thr37−His41−His118 hydrogen bond bridge (Figure 1). This finding strongly suggests that the hydrogen bond bridge is important in maintaining the high catalytic efficiency of SOD. Figure 8 shows the subunit architecture of bovine SOD revealed by X-ray diffraction (*8*). Eight β-strands arranged in a Greek key fold form a β-barrel, and His41 is positioned at an opening of the β-barrel. The Thr37−His41−His118 hydrogen bond bridge connects a short loop crossing the opening of the β-barrel (Thr37) to an edge of the β-barrel wall (His118). A peptide bond further links Thr37 to Leu36, whose side chain is in van der Waals contact with His41 and serves as a hydrophobic plug filling the gap created by Val14, Ile33, Val85, Ala87, Ala93, Val117, and Leu142 at the opening of the β-barrel (*40*, *62*−*64*). The hydrophobic interactions of Leu36 with the surrounding residues are considered to play an important role in stabilizing the compact Greek key fold of the β-barrel (*34*). On the other hand, the hydrogen bond from His41 to His118 is further extended to Arg141 through two planar amide linkages and an N−H···O═C hydrogen bond (Figure 8). The positively charged side chain of Arg141 stretches out toward the active site to dock superoxide (Figure 8) and has been shown to be essential for catalysis by chemical modification and site-directed mutagenesis (*22*, *23*). Thus, His41 indirectly connects the structurally important residue, Leu36, with the catalytically essential residue, Arg141. Disruption of the Thr37−His41−His118 hydrogen bond bridge would alter the positions and/or orientations of the Leu36 and Agr141 side chains, leading to a distortion of the SOD structure from that most suitable for catalytic reactions. It is highly probable that His41 plays a crucial role in stabilizing the compact structure of the β-barrel and in assisting the correct arrangement of the Arg141 side chain with respect to the active Cu center.

Electrostatic Loop. The loop region between His118 and Arg141 is called the "electrostatic loop" because it contains four highly conserved charged residues (Lys120, Glu130, Glu131, and Lys134). These charged residues were postulated to assist highly efficient catalytic reactions of SOD by attracting and steering superoxide anions toward the Cu site

by long-range electrostatic interactions (*24*−*31*). In this context, the deactivation of SOD at pH 9.5 was interpreted as arising from deprotonation of Lys120 and/or Lys134 (*24*, *27*−*31*). However, recent mutagenesis data have demonstrated that the electrostatic loop is not essential for high catalytic efficiency of SOD (*32*, *33*). In this study, we have shown that the deactivation at pH 9.5 can be linked with the deprotonation of His41. Although it is possible that Lys120 and Lys134 also have pK_a values around pH 9.5, the effect of Lys deprotonation on the catalytic activity would not be dominant, at least under physiological ionic strength conditions where the present UV Raman investigations were performed.

Comparison with Human SOD. Human SOD shares a high degree of sequence homology (83%) with bovine SOD (*34*), and its three-dimensional structure and catalytic properties are very similar to those of bovine SOD (*58*, *59*, *65*). His43 of human SOD forms a hydrogen bond bridge between the main chain C═O groups of Thr39 and His120. (The residue numbers differ from those of bovine SOD because of the insertion of two residues after Asp25.) The side chain of Leu38 points toward the core of the β-barrel to plug up a hydrophobic hole created by the side chains of Val14, Ile35, Val119, and others (*58*, *59*). It also appears that catalytically essential Arg143 is linked to His43 through a chain of amide and hydrogen bonds. His43 in human SOD seems to play the same catalytic and structural role as His41 does in bovine SOD. A recent X-ray diffraction study on the His43 → Arg mutant of human SOD has shown that the Arg side chain is hydrogen bonded with Thr39 but not with His120 (*59*). Concomitantly, the mutation causes a 60% reduction in dismutase activity (*58*), which is comparable to that observed for bovine SOD upon disruption of the His41−His118 hydrogen bond at pH 9.5 (pD 9.4). The importance of the His41 (His43) hydrogen bonding in catalytic activity is also suggested by the data on human SOD.

SOD has been implicated in amyotrophic lateral sclerosis (ALS), which is one of the most common neurodegenerative disorders in humans and is characterized by the progressive loss of motor neurons of the brain and spinal cord, leading to eventual paralysis and death of affected individuals. Various point mutations of SOD have been identified in ∼20% of familial ALS (FALS) patients, and mutation of SOD has been proposed to be a possible cause of ALS (*58*, *64*, *66*, *67*). Clusters of FALS-related point mutations are found around the β-barrel opening and the intersubunit contact regions (*59*). His43 takes the central position of such a cluster at one opening of the β-barrel, and the His43 → Arg mutation has been identified in patients of FALS (*58*, *66*, *67*). In addition to the reduced activity described above, the His43 → Arg mutant is characterized by an increased propensity for fibrous aggregation resulting from a reduced stability of the protein structure, including the β-barrel domain (*59*). The structural instability introduced by the His43 → Arg mutation in human SOD is in line with the UV Raman finding presented here that solvent accessibility to the β-barrel interior of bovine SOD is enhanced by the disruption of the Thr37−His41−His118 hydrogen bond bridge. Structural and biochemical data available for bovine and human SOD are fully consistent with a crucial role of the conserved, metal-free His residue (His41 in bovine SOD and His43 in human SOD) in the catalytic activity and structural stability of the antioxidant enzyme.

REFERENCES

1. McCord, J. M., and Fridovich, I. (1969) Superoxide dismutase. An enzymic function for erythrocuprein (hemocuprein), *J. Biol. Chem. 244*, 6049−6055.
2. Fridovich, I. (1975) Superoxide dismutases, *Annu. Rev. Biochem. 44*, 147−159.
3. Fridovich, I. (1995) Superoxide radical and superoxide dismutases, *Annu. Rev. Biochem. 64*, 97−112.
4. Cheeseman, K. H., and Slater, T. F. (1993) An introduction to free radical biochemistry, *Br. Med. Bull. 49*, 481−493.
5. McCord, J. M. (2002) Superoxide dismutase in aging and disease: an overview, *Methods Enzymol. 349*, 331−341.
6. Maier, C. M., and Chan, P. K. (2002) Role of superoxide dismutases in oxidative damage and neurodegenerative disorders, *Neuroscientist 8*, 323−334.
7. Noor, R., Mittal, S., and Iqbal, J. (2002) Superoxide dismutase: applications and relevance to human diseases, *Med. Sci. Monit. 8*, RA210−RA215.
8. Tainer, J. A., Getzoff, E. D., Beem, K. M., Richardson, J. S., and Richardson, D. C. (1982) Determination and analysis of the 2 Å structure of copper, zinc superoxide dismutase, *J. Mol. Biol. 160*, 181−217.
9. Ferraroni, M., Rypniewski, W. R., Bruni, B., Orioli, P., and Mangani, S. (1998) Crystallographic determination of reduced bovine superoxide dismutase at pH 5.0 and of anion binding to its active site, *J. Biol. Inorg. Chem. 3*, 411−422.
10. Hough, M. A., Strange, R. W., and Hasnain, S. S. (2000) Conformational variability of the Cu site in one subunit of bovine Cu,Zn superoxide dismutase: the importance of mobility in the Glu119−Leu142 loop region for catalytic function, *J. Mol. Biol. 302*, 231−241.
11. Rypniewski, W. R., Mangani, S., Bruni, B., Orioli, P. L., Casati, M., and Wilson, K. S. (1995) Crystal structure of reduced bovine erythrocyte superoxide dismutase at 1.9 Å resolution, *J. Mol. Biol. 251*, 282−296.
12. Hough, M. A., and Hasnain, S. S. (1999) Crystallographic structures of bovine copper−zinc superoxide dismutase reveal asymmetry in two subunits: functionally important three and five coordinate copper sites captured in the same crystal, *J. Mol. Biol. 287*, 579−592.
13. Tainer, J. A., Getzoff, E. D., Richardson, J. S., and Richardson, D. C. (1983) Structure and mechanism of copper, zinc superoxide dismutase, *Nature 306*, 284−287.
14. Hart, P. J., Balbirnie, M. M., Ogihara, N. L., Nersissian, A. M., Weiss, M. S., Valentine, J. S., and Eisenberg, D. (1999) A structure-based mechanism for copper−zinc superoxide dismutase, *Biochemistry 38*, 2167−2178.
15. Bertini, I., Luchinat, C., and Monnanni, R. (1985) Evidence of the breaking of the copper-imidazolate bridge in copper/cobalt-substituted superoxide dismutase upon reduction of the copper-(II) centers, *J. Am. Chem. Soc. 107*, 2178−2179.
16. Murphy, L. M., Strange, R. W., and Hasnain, S. S. (1997) A critical assessment of the evidence from XAFS and crystallography for the breakage of the imidazolate bridge during catalysis in Cu,Zn superoxide dismutase, *Structure 5*, 371−379.
17. Ascone, I., Castañer, R., Tarricone, C., Bolognesi, M., Stroppolo, M. E., and Desideri, A. (1997) Evidence of His61 imidazolate bridge rupture in reduced crystalline Cu,Zn superoxide dismutase, *Biochem. Biophys. Res. Commun. 241*, 119−121.
18. Hashimoto, S., Ono, K., and Takeuchi, H. (1998) UV Raman scattering from metal-coordinating histidine residues in Cu,Zn-superoxide dismutase, *J. Raman Spectrosc. 29*, 969−975.
19. Ratilio, G., Bray, R. C., and Fielden, E. M. (1972) A pulse radiolysis study of superoxide dismutase, *Biochim. Biophys. Acta 268*, 605−609.
20. Klug, D., Rabani, J., and Fridovich, I. (1972) A direct demonstration of the catalytic action of superoxide dismutase through the use of pulse radiolysis, *J. Biol. Chem. 247*, 4839−4842.
21. Argese, E., Viglino, P., Rotilio, G., Scarpa, M., and Rigo, A. (1987) Electrostatic control of the rate-determining step of the copper, zinc superoxide dismutase catalytic reaction, *Biochemistry 26*, 3224−3228.

22. Malinowski, D. P., and Fridovich, I. (1979) Chemical modification of arginine at the active site of the bovine erythrocyte superoxide dismutase, *Biochemistry 18*, 5909−5917.
23. Fisher, C. L., Cabelli, D. E., Tainer, J. A., Hallewell, R. A., and Getzoff, E. D. (1994) The role of arginine 143 in the electrostatics and mechanism of Cu,Zn superoxide dismutase: computational and experimental evaluation by mutational analysis, *Proteins 19*, 24−34.
24. Cudd, A., and Fridovich, I. (1982) Electrostatic interactions in the reaction mechanism of bovine erythrocyte superoxide dismutase, *J. Biol. Chem. 257*, 11443−11447.
25. Getzoff, E. D., Tainer, J. A., Weiner, P. K., Kollman, P. A., Richardson, J. S., and Richardson, D. C. (1983) Electrostatic recognition between superoxide and copper, zinc superoxide dismutase, *Nature 306*, 287−290.
26. Getzoff, E. D., Cabelli, D. E., Fisher, C. L., Parge, H. E., Viezzoli, M. S., Banci, L., and Hallewell, R. A. (1992) Faster superoxide dismutase mutants designed by enhancing electrostatic guidance, *Nature 358*, 347−351.
27. Argese, E., Girotto, R., and Orsega, E. F. (1993) Comparative kinetic study between native and chemically modified Cu,Zn superoxide dismutases, *Biochem. J. 292*, 451−455.
28. O'Neill, P., Davies, S., Fielden, E. M., Calabrese, L., Capo, C., Marmocchi, F., Natoli, G., and Rotilio, G. (1988) The effects of pH and various salts upon the activity of a series of superoxide dismutases, *Biochem. J. 251*, 41−46.
29. Polticelli, F., O'Neill, P., Costanzo, S., Lania, A., Rotilio, G., and Desideri, A. (1995) Identification of the residues responsible for the alkaline inhibition of the activity of Cu,Zn superoxide dismutase: a study of native and chemically modified enzymes, *Arch. Biochem. Biophys. 321*, 123−126.
30. Polticelli, F., Battistoni, A., O'Neill, P., Rotilio, G., and Desideri, A. (1996) Identification of the residues responsible for the alkaline inhibition of Cu,Zn superoxide dismutase: a site-directed mutagenesis approach, *Protein Sci. 5*, 248−253.
31. Fisher, C. L., Cabelli, D. E., Hallewell, R. A., Beroza, P., Lo, T. P., Getzoff, E. D., and Tainer, J. A., (1997) Computational, pulse-radiolytic, and structural investigations of lysine-136 and its role in the electrostatic triad of human Cu,Zn superoxide dismutase, *Proteins 29*, 103−112.
32. Polticelli, F., Battistoni, A., O'Neill, P., Rotilio, G., and Desideri, A. (1998) Role of the electrostatic loop charged residues in Cu,-Zn superoxide dismutase, *Protein Sci. 7*, 2354−2358.
33. Ciriolo, M., Battistoni, A., Falconi, M., Filomeni, G., and Rotilio, G. (2001) Role of the electrostatic loop of Cu,Zn superoxide dismutase in the copper uptake process, *Eur. J. Biochem. 268*, 737−742.
34. Bordo, D., Djinović, K., and Bolognesi, M. (1994) Conserved patterns in the Cu,Zn superoxide dismutase family, *J. Mol. Biol. 238*, 366−386.
35. Zhao, X., Wang, D., and Spiro, T. G. (1998) A UV resonance Raman monitor of histidine protonation in proteins: Bohr protons in hemoglobin, *J. Am. Chem. Soc. 120*, 8517−8518.
36. Zhao, X., Chen, R., Raj, V., and Spiro, T. G. (2001) Assignment of the 1511 cm^{-1} UV resonance Raman marker band of hemoglobin to tryptophan, *Biopolymers 62*, 158−162.
37. Okada, A., Miura, T., and Takeuchi, H. (2001) Zinc- and pH-dependent conformational transition in a putative interdomain linker region of the influenza virus matrix protein M1, *Biochemistry 40*, 6053−6060.
38. Wu, Q., Li, F., Wang, W., Hecht, M. H., and Spiro, T. G. (2002) UV Raman monitoring of histidine protonation and H−^{2}H exchange in plastocyanin, *J. Inorg. Biochem. 88*, 381−387.
39. Takeuchi, H. (2003) Raman structural markers of tryptophan and histidine side chains in proteins, *Biopolymers 72*, 305−317.
40. Banci, L., Bertini, I., Cramaro, F., Del Conte, R., and Viezzoli, M. S. (2002) The solution structure of reduced dimeric copper zinc superoxide dismutase. The structural effects of dimerization, *Eur. J. Biochem. 269*, 1905−1915.
41. Beauchamp, C., and Fridovich, I. (1971) Superoxide dismutase: improved assays and an assay applicable to acrylamide gels, *Anal. Biochem. 44*, 276−287.
42. Sundius, T. (1973) Computer fitting of Voigt profiles to Raman lines, *J. Raman Spectrosc. 1*, 471−488.
43. Thompson, W. J. (1993) Numerous neat algorithms for the Voigt profile function, *Comput. Phys. 7*, 627−631.
44. Harada, I., and Takeuchi, H. (1986) Raman and ultraviolet resonance Raman spectra of proteins and related compounds, in *Spectroscopy of Biological Systems* (Clark, R. J. H., and Hester, R. E., Eds.) pp 113−175, Wiley, New York.
45. Austin, J. C., and Spiro, T. G. (1993) Ultraviolet resonance Raman studies of proteins and related model compounds, in *Biomolecular Spectroscopy, Part A* (Clark, R. J. H., and Hester, R. E., Eds.) pp 55−127, Wiley, New York.
46. Hashimoto, S., Ohsaka, S., Takeuchi, H., and Harada, I. (1989) Ultraviolet resonance Raman spectra of copper, zinc-superoxide dismutase: detection of an imidazolate bridge between the metal ions in solution, *J. Am. Chem. Soc. 111*, 8926−8928.
47. Zhao, X., Wang, D., and Spiro, T. G. (1998) Detection of metal-bound histidine in ultraviolet resonance Raman spectra: superoxide dismutase, *Inorg. Chem. 37*, 5414−5415.
48. Wang, D., Zhao, X., Vargek, M., and Spiro, T. G. (2000) Metal-bound histidine modes in UV resonance Raman spectra of Cu, Zn superoxide dismutase, *J. Am. Chem. Soc. 122*, 2193−2199.
49. Gregory, R. B., and Rosenberg, A. (1986) Protein conformational dynamics measured by hydrogen isotope exchange techniques, *Methods Enzymol. 131*, 448−508.
50. Tu, A. T. (1986) Peptide backbone conformation and microenvironment of protein side chain, in *Spectroscopy of Biological Systems* (Clark, R. J. H., and Hester, R. E., Eds.) pp 47−112, Wiley, New York.
51. Hill, A. V. (1910) The possible effects of the aggregation of the molecules of haemoglobin on its oxygen dissociation curve, *J. Physiol. 40*, 4−7.
52. Fersht, A. (1977) *Enzyme Structure and Mechanism*, Freeman, New York.
53. Cass, A. E. G., Allen, H., Hill, O., Smith, B. E., Bannister, J. V., and Bannister, W. H. (1977) Investigation of the structure of bovine erythrocyte superoxide dismutase by proton nuclear magnetic resonance spectroscopy, *Biochemistry 16*, 3061−3066.
54. Desideri, A., Polticelli, F., Falconi, M., Sette, M., Ciriolo, M. A., Paci, M., and Rotilio, G., (1993) Electrostatic recognition in redox copper proteins: a ^{1}H NMR study of the protonation behavior of His 19 in oxidized and reduced Cu,Zn superoxide dismutase, *Arch. Biochem. Biophys. 301*, 244−250.
55. Itabashi, M., and Itoh, K. (1980) Raman scattering study on coordination structure of Cu(II)-L-Histidine(1:2) in aqueous solution, *Bull. Chem. Soc. Jpn. 53*, 3131−3137.
56. Ashikawa, I., and Itoh, K. (1979) Raman spectra of polypeptides containing L-histidine residues and tautomerism of imidazole side chain, *Biopolymers 18*, 1859−1876.
57. Allen, H., Hill, O., Lee, W.-K., Bannister, J. V., and Bannister, W. H. (1980) Investigation of human erythrocyte superoxide dismutase by ^{1}H nuclear-magnetic-resonance spectroscopy, *Biochem. J. 185*, 245−252.
58. Deng, H. X., Hentati, A., Tainer, J. A., Iqbal, Z., Cyabyab, A., Hang, W.-Y., Getzoff, E. D., Hu, P., Herzfeldt, B., Roos, R. P., Warner, C., Deng, G., Soriano, E., Smyth, C., Parge, H. E., Ahmed, A., Roses, A. D., Hallewell, R. A., Pericak-Vance, M. A., and Siddique, T. (1993) Amyotrophic lateral sclerosis and structural defects in Cu,Zn superoxide dismutase, *Science 261*, 1047−1051.
59. DiDonato, M., Craig, L., Huff, M. E., Thayer, M. M., Cardoso, R. M. F., Kassmann, C. J., Lo, T. P., Bruns, C. K., Powers, E. T., Kelly, J. W., Getzoff, E. D., and Tainer, J. A. (2003) ALS mutants of human superoxide dismutase form fibrous aggregates via framework destabilization, *J. Mol. Biol. 332*, 601−615.
60. Edgcomb, S. P., and Murphy, K. P. (2002) Variability in the pK_a of histidine side chains correlates with burial within proteins, *Proteins 49*, 1−6.
61. Tishmack, P. A., Bashford, D., Harms, E., and Van Etten, R. L. (1997) Use of ^{1}H NMR spectroscopy and computer simulations to analyze histidine pK_a changes in a protein tyrosine phosphatase: experimental and theoretical determination of electrostatic properties in a small protein, *Biochemistry 36*, 11984−11994.
62. Parge, H. E., Hallewell, R. A., and Tainer, J. A. (1992) Atomic structures of wild-type and thermostable mutant recombinant human Cu,Zn superoxide dismutase, *Proc. Natl. Acad. Sci. U.S.A. 89*, 6109−6113.
63. Deng, H. X., Tainer, J. A., Mitsumoto, H., Ohnishi, A., He, X., Hung, W. Y., Zhao, Y., Juneja, T., Hentati, A., and Siddique, T. (1995) Two novel SOD1 mutations in patients with familial amyotrophic lateral sclerosis, *Hum. Mol. Genet. 4*, 1113−1116.

64. Rakhit, R., Cunningham, P., Furtos-Matei, A., Dahan, S., Qi, X.-F., Crow, J. P., Cashman, N. R., Kondejewski, L. H., and Chakrabartty, A. (2002) Oxidation-induced misfolding and aggregation of superoxide dismutase and its implications for amyotrophic lateral sclerosis, *J. Biol. Chem. 277*, 47551−47556.
65. Bertini, I., Banci, L., Luchinat, C., Bielski, B. H. J., Cabelli, D. E., Mullenbach, G. T., and Hallewell, R. A. (1989) An investigation of a human erythrocyte SOD modified at position 137, *J. Am. Chem. Soc. 111*, 714−719.
66. Rosen, D. R., Siddique, T., Patterson, D., Figlewicz, D. A., Sapp, P., Hentati, A., Donaldson, D., Goto, J., O'Regan, J., Deng, H. X., Rahmani, Z., Krizus, A., McKenna-Yasek, D., Cayabyab, A., Gatson, S. M., Berger, R., Tanzi, R. E., Halperin, J. J., Herzfeldt, B., Van der Bergh, R., Hung, W.-Y., Bird, T., Deng, G., Mulder, D. W., Smyth, C., Laing, N. G., Soriano, E., Pericak-Vance, M. A., Haines, J., Rouleau, G. A., Gusella, J. S., Horvitz, H. R., and Brown, R. H., Jr. (1993) Mutations in Cu/Zn superoxide dismutase gene are associated with familial amyotrophic lateral sclerosis, *Nature 362*, 59−62.
67. Cudkowicz, M. E., McKenna-Yasek, D., Sapp, P. E., Chin, W., Geller, B., Hayden, D. L., Schoenfeld, D. A., Hosler, B. A., Horvitz, H. R., and Brown, R. H. (1997) Epidemiology of mutations in superoxide dismutase in amyotrophic lateral sclerosis, *Ann. Neurol. 41*, 210−221.

BI049767K